Mechanism of compensation of aberrations in the human eye

Juan Tabernero,* Antonio Benito, Encarna Alcón, and Pablo Artal

Laboratorio de Óptica, Departamento de Física, Universidad de Murcia, Campus de Espinardo, (Edificio CiOyN), 30071 Murcia, Spain

**Corresponding author: juant@um.es*

Received April 18, 2007; revised August 1, 2007; accepted August 5, 2007; posted August 8, 2007 (Doc. ID 82196); published September 20, 2007

We studied the mechanism of compensation of aberrations within the young human eye by using experimental data and advanced ray-tracing modeling. Corneal and ocular aberrations along with the alignment properties (angle kappa, lens tilt, and decentration) were measured in eyes with different refractive errors. Predictions from individualized ray-tracing optical models were compared with the actual measurements. Ocular spherical aberration was, in general, smaller than corneal spherical aberration without relation to refractive error. However, horizontal coma compensation was found to be significantly larger for hyperopic eyes where angle kappa tended to also be larger. We propose a simple analytical model of the relationship between the corneal coma compensation effect with the field angle and corneal and crystalline shape factors. The actual shape factors corresponded approximately to the optimum shapes that automatically provide this coma compensation. We showed that the eye behaves as an aplanatic optical system, an optimized design solution rendering stable retinal image quality for different ocular geometries.

OCIS codes: 330.0330, 330.4460, 220.1000, 220.2740.

1. INTRODUCTION

The optics of the human eye impose the first physical limit to visual perception. A good quality retinal image is required for good vision. The human eye is a relatively simple optical device with only two elements: the cornea and the crystalline lens. However, we do not yet have a complete understanding of the details of the optical properties of the eye. In recent years, the application of new technology has been instrumental to further study the ocular optics. One of the most significant advancements was to recognize that in the normal young eye the optical properties of the two ocular components were somehow tuned to produce an improved overall image quality. In particular, the corneal spherical aberration (SA) tends to be balanced by the young crystalline lens [1–3]. Normal aging disrupts this balance [4], mainly due to the change of the lens' spherical aberration from negative to positive values [5], while corneal SA remains approximately stable with age [6]. The mechanism responsible for the compensation of SA may have a straightforward optical formulation in terms of the lens structural parameters (asphericity, gradient index parameters, etc…). These results had important clinical implications [7,8] leading to a new type of aspheric intraocular lenses (IOLs) designed to compensate for the average values of corneal SA [9,10].

Other aberration terms, such as coma, also showed a systematic balance between the cornea and the internal optics of the eye. In particular, the compensation of horizontal coma has been previously demonstrated [11,12]. It was found that the degree of compensation of corneal coma increases with the distance between the pupillary reflex and the center of the entrance pupil of the eye. This distance is directly proportional to the angle kappa of the eye. After the definition of Le Grand [13], this is the angular distance between the line of sight and the pupillary axis (see Fig. 1), although in the literature this is also often referred to as angle lambda [14]. Typically, angle kappa is larger in hyperopic eyes [13], and therefore, horizontal coma was found to be more compensated for those subjects than for myopic eyes. As an interesting application of this result, we have recently proposed a new IOL designed to compensate for corneal coma [17].

The imaging properties of the eye, that is to say its aberration structure, are produced by the shape of the surfaces, their location, relative alignment, and the distribution of refractive indexes of the ocular media. Different authors used instruments to obtain information on the relative alignment of cornea, lens, and fovea by using Purkinje images [18–21]. The aberrations of the cornea can be estimated from corneal topography data [22,23] and the aberrations of the complete eye can be measured with wavefront sensors (Hartmann–Shack type sensors [24,25] are the most widely used). The incorporation of all these new experimental data of the living eye into advanced optical modeling [26] would permit a complete understanding of the mechanism of the compensation of the aberration.

In this context, this paper presents a complete study of the causes of the compensation of aberrations of the young human eye. A detailed set of measurements of different optical parameters was performed in a group of young subjects, covering a large refractive error range, from myopes to hyperopes. By individualized optical modeling, the aberrations for each eye were predicted and then compared with the actual data. These results lead, for what we believe is the first time, to a detailed expla-

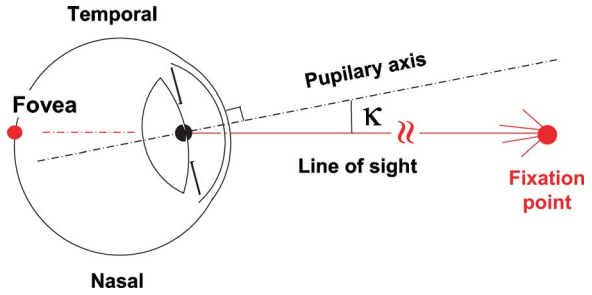

Fig. 1. (Color online) Definition of angle kappa, line of sight, and pupillary axis.

nation of the causes of the aberration structure of the normal eye, revealing the mechanisms of aberration compensation.

2. MATERIALS AND METHODS

A. Subjects, Instrumentation and Measurements

We selected 18 subjects (between the ages of 20 and 26) to participate in this study (mean 22.3 years, standard deviation 2.0 years) with refractive errors between −8.5 D to +4 D. Four of them were nearly emmetropes, eight were myopes (from −8.5 to −2.75 D) and six were hyperopes (from +1 to +4 D). The complete measurement session consisted of the assessment of the optical alignment of the ocular components: lens tilt and decentration with respect to the line of sight and angle kappa, using our own developed research prototype based on recording Purkinje images [19]. The corneal aberrations were estimated with a ray-tracing procedure [23] from the shape of the cornea measured with a clinical topographer (Atlas, Zeiss Meditec). Axial length and anterior chamber depth were assessed using a low coherence interferometry instrument (IOL Master, Zeiss Meditec). The wavefront aberrations for the complete eye were measured with our own Hartmann–Shack wavefront sensor [25]. All the measurements were performed under normal viewing conditions without pharmacological pupil dilation. Practices and research adhered to the tenets of the Declaration of Helsinki. Informed consent was obtained from each subject after explanation of the nature and possible consequences of the procedures.

The assessment of lens tilt and decentration using Purkinje images was performed using a custom-developed clinical prototype. It follows a method that has already been explained in detail elsewhere [21]. Briefly, Purkinje images were recorded at the same time that the subject performed nine controlled fixations (more eccentric targets were situated at 5° with respect to the line of sight). The distances from each Purkinje reflection to the center of the entrance pupil of the eye were adjusted as a linear function of the fixation angle. The overlapping point between both lens reflections was interpolated from those fittings. This position indicates the lens' optical axis. The angular distance that the line of sight must rotate to locate this alignment point was used to estimate lens tilt with respect to the line of sight. Also, the position from the overlapping point to the center of the entrance pupil can be considered as an estimation of the lens decentration with respect to the pupil center. The angular difference between the line of sight and the pupillary axis can be estimated from the extrapolated ocular rotation, which makes the corneal reflex and the center of the entrance pupil overlap (see [21] for additional details of the procedure that followed the measuring of the ocular angles).

The ocular wavefront aberrations were measured using a near-infrared Hartmann–Shack wavefront sensor adapted to the clinical environment. This system has more than 220 microlenses over a 5 mm pupil area (the size of each microlens on the eye's pupil is 0.2 mm) and it has a high-dynamic range allowing us to measure large aberrations with enough accuracy. The corneal surface was obtained from videokeratoscopy measurements. The elevations provided by corneal topography were imported into ray-tracing software to calculate the wavefront aberrations associated with the corneal surface. Both ocular and corneal wavefront aberrations were centered on the entrance pupil of the eye and expressed as a Zernike polynomial expansion. Internal aberrations were then estimated from the direct subtraction of the corneal aberrations to the total aberrations, neglecting the small stop-shift effect between cornea and lens aberrations (assuming that aberrations remain very similar along small axial distances).

B. Individualized Eye Models

The experimental data collected, corneal shape, eye geometrical distances, and surface alignments, were used to build up the individualized eye models [26]. The cornea was approximated by one surface, exporting the elevation data into the ray-tracing software. Part of the effect of the back corneal surface was considered using an effective index of refraction for the cornea. To correct for the misalignment between the videokeratoscopy data centration (the topography data was centered on the corneal reflex) and the entrance pupil center, we used the information provided by the first Purkinje image taken with our instrument. Therefore, the corneal surface used for the calculations was the corneal zone centered over the entrance pupil. Since the center of the entrance pupil was also used for centering the ocular wavefront measurements, no lateral shift was induced when comparing both measurements; the common axis for each individualized model was the line of sight (connecting the center of the entrance pupil to the fixation stimulus).

The modeling of the crystalline lens presents more methodological problems because we did not have access to complete information *in vivo*. The only objective information obtained from the lens was the alignment and the axial position of the anterior surface. A simple rotationally symmetrical lens model approach was proposed, with the values of internal SA adjusted to those measured by direct subtraction of the corneal SA to the ocular SA. The hypothesis of null intrinsic lens aberrations was implicit in the formulation of this lens model (with the exception of spherical aberration). However, this model was expected to account for all angular generated aberrations, such as coma. To reproduce the most similar lens structure, the lens power was also adjusted to account for the refractive error of each subject.

To fit all these lens features within the experimental data, an optimization strategy based on changing some of

the lens parameters was designed. However, the solution to the optimization procedure in a multivariate space may be very dependent on the starting point. In this work, lens parameters of two average model eyes were used as the starting point for the procedure: the Gullstrand (unaccommodated) [13] and the Liu–Brennan [27] eye models. The crystalline lens from the Gullstrand eye model is an average spherical lens, while the lens from the Liu–Brennan eye model includes asphericity in both surfaces, and a parabolic gradient index profile that reproduces the average measurement of ocular SA. In the first case, the variables that were used to determine a possible solution were the radii of curvature and asphericity. while in the second case a more sophisticated lens was obtained also using the parabolic parameters of the gradient index as variables. Therefore, for each subject's eye, two different lens models were used. The data related to misalignments were also directly incorporated into the calculations. However, different configurations with the alignment parameters were also explored to investigate their relative influence into the eye's aberrations. Alternative modeling that only incorporated horizontal lens tilt (neglecting any other alignment parameter) and centered lenses was also considered. In each eye, the wavefront aberrations were obtained by tracing finite rays through for different model configurations. The results were compared with those measured in each eye by the Hartmann–Shack wavefront sensor.

3. RESULTS

A. Aberrations and Alignment Data

Figure 2 shows the measured aberrations [total root-mean-squared (rms), vertical and horizontal coma, and SA] of the ocular components: cornea, lens (internal), and complete eye, as a function of the refractive error for each subject. Corneal SA is compensated by the lens, producing an eye with slightly positive SA. This compensation of SA does not depend upon the refractive state. It is interesting to note that the only statistically significant correlation between an aberration term and refractive error was found in the cases of corneal and internal horizontal coma. In Fig. 2, the sign for horizontal coma was changed for the right eyes to better visualize the compensation effect. While the ocular horizontal coma was not statistically correlated with the refractive error, remaining similar for myopic and hyperopic subjects, a positive tendency with refractive error was clearly noticeable for horizontal corneal coma ($R=0.70$, $p=0.0012$). In addition, a negative correlation of internal coma with refractive error was also observed ($R=-0.62$, $p=0.0062$). No statistically significant correlations were observed for vertical coma and refractive error. Moreover, the ocular values of the average higher-order rms error remained similar for both myopic to hyperopic eyes, while a positive statistically significant correlation was found for the corneal higher-order rms ($R=0.63$, $p=0.05$) and internal higher-order rms ($R=0.49$, $p=0.039$).

Figure 3 summarizes the results from Fig. 2, grouping the subjects by refractive error. The compensation of coma (right bar of each group) increased with refractive error while neither the compensated SA (central bar) nor the

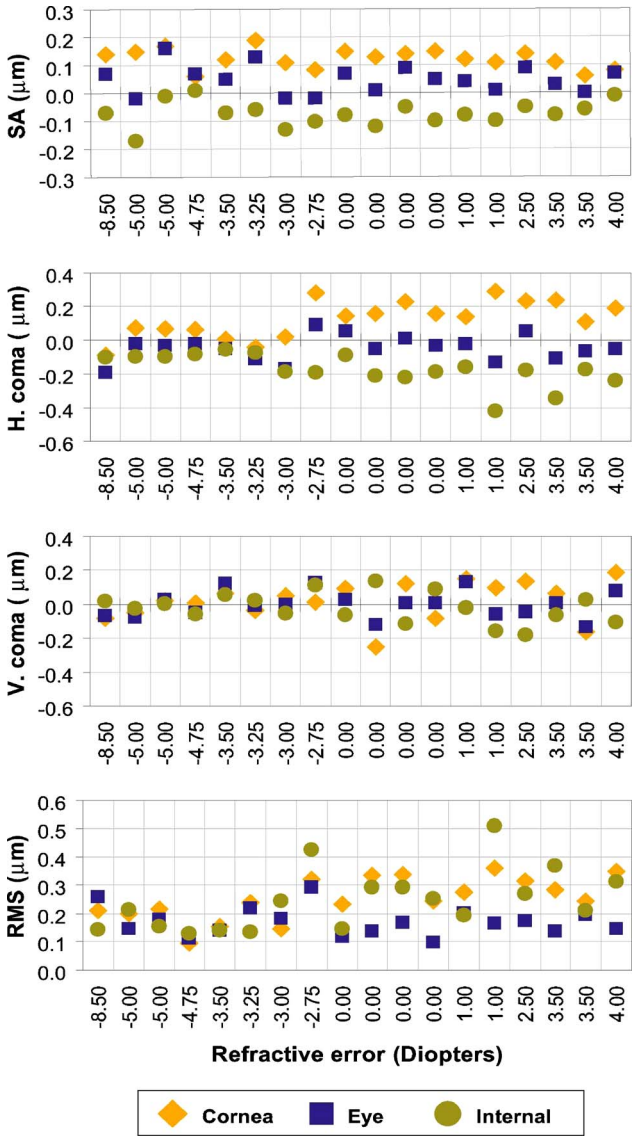

Fig. 2. (Color online) Spherical aberration, coma, and higher-order root-mean-squared wavefront error for the cornea, eye, and internal components of all the subjects included in this work, sorted by the refractive error, from the more myopic to the more hyperopic eye.

ocular higher-order rms (left bar) changed significantly with refraction. Figure 4 presents the average higher-order aberration maps for the myopic and the hyperopic groups. To obtain these average wavefronts, data of left and right eyes were averaged changing the sign of Zernike terms with odd symmetry on the y-axis for the right eyes. The compensation of corneal horizontal coma by the crystalline lens is clearly noticed in the hyperopic subjects. In the myopic group, although the corneal SA compensation effect is still noticeable, the compensation of coma is clearly reduced.

The alignment values for this group of eyes are depicted in Fig. 5 as polar graphs. Angle kappa and lens tilt with respect to the line of sight shows a horizontal tendency, with the pupillary axis oriented temporally in the object space with respect to the line of sight. Furthermore, the values for these two parameters were clearly interrelated ($R=0.73$, $p=0.0006$). Lens tilt with respect to

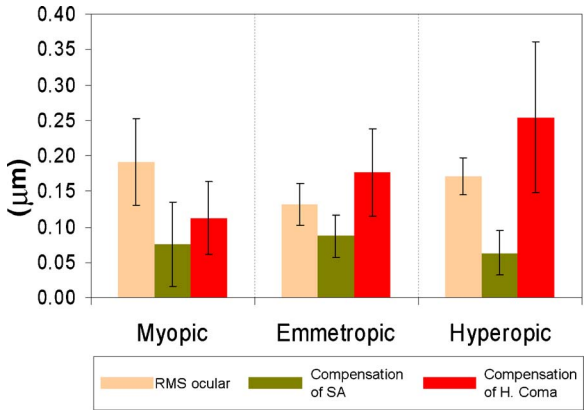

Fig. 3. (Color online) Average ocular rms, compensated coma, and compensated spherical aberration grouping the subjects into myopic, emmetropic, and hyperopic eyes. Error bars represent standard deviation from the average.

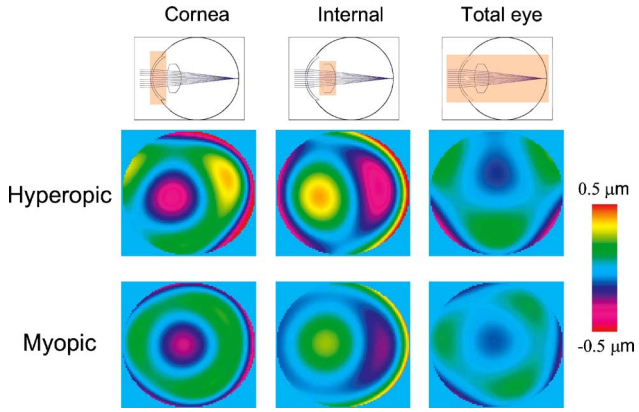

Fig. 4. (Color online) Average higher-order wavefront maps for the hyperopic and myopic group. Corneal internal and ocular aberration maps are shown in each column separately.

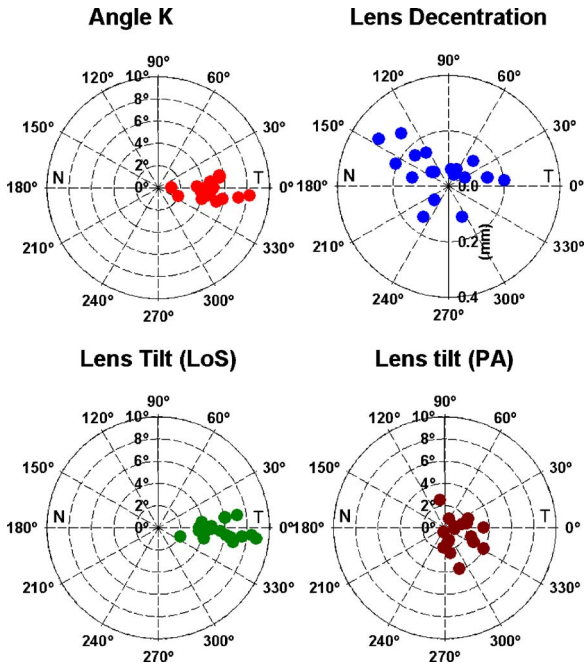

Fig. 5. (Color online) Alignment data measured for all the subjects included in this study.

the pupillary axis was also orientated with a temporal trend in the object space, but with no horizontal or vertical predominant direction. Lens decentration with respect to the entrance pupil center did not show any special orientation tendency, being in general small, with a mean radial magnitude of 0.13 mm (standard deviation = 0.07 mm). The lens alignment properties did not show any statistically significant correlation with the refractive error, with the exception of the horizontal component of the lens tilt with respect to the line of sight ($R=0.54$, $p=0.02$). Myopic eyes tended to have a slightly smaller value of horizontal lens tilt (Fig. 6). Due to this relationship, it is interesting to study how the horizontal components of tilt were related to the actual values of horizontal coma. Figure 7 shows the relationship between the measured horizontal component of angle kappa and the horizontal component of coma for the different optical components of the eye. Corneal coma tended to increase with the horizontal value of angle kappa ($R=0.83$, $p<0.0001$). The slope of the linear fit was 0.028 μm per degree of angle kappa. A correlation of the ocular horizontal coma with the angle kappa was also observed ($R=-0.50$, $p=0.035$) but with a smaller slope (−0.008 μm per degree) and without the strong statistical significant of the corneal coma. From the subtraction of both values, the opposite correlation was found for internal coma ($R=0.90$, $p<0.00001$) with a slope of −0.037 μm of coma per degree.

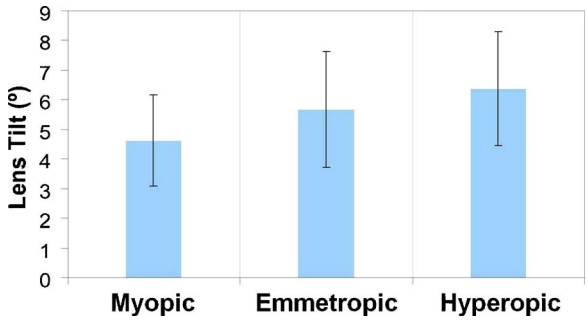

Fig. 6. (Color online) Lens tilt with respect to the line of sight for the refractive groups in the study.

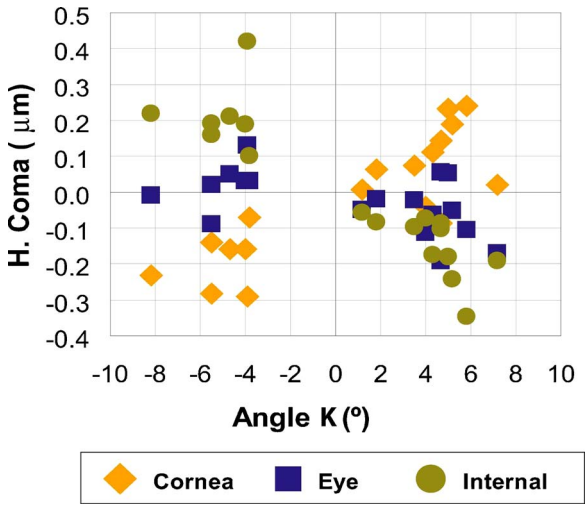

Fig. 7. (Color online) Relationship between angle kappa and horizontal coma for the whole eye, cornea, and internal optics.

B. Comparison of Modeling and Measurement Data

The agreement between the aberrations predicted by the different ocular models and the actual measurements from the HS sensor were assessed in terms of the correlation levels. Figure 8 illustrates the impact of lens alignment on the prediction of horizontal coma. The diamond shape points represent the value of horizontal coma obtained from an ocular model whose crystalline lens incorporated all the actual alignment data (tilt and decentration) as a function of the measured value of horizontal coma. The crystalline lens in the model was optimized to match the spherical aberration value measured, using the radii and asphericity in both surfaces as variables, with the Gullstrand lens model as the starting point for the procedure. The straight line represented the linear fit of the predicted versus the measured values of coma ($R=0.79$, $p=0.0001$). The squares symbols represent the same case as before, but they incorporate only the values of horizontal tilt to the crystalline lens and alignment properties. Vertical tilts with respect to the line of sight and lens decentration with respect to the pupil center were neglected in this case. The dashed line ($R=0.83$, $p<0.0001$) showed the linear correlation with the measured values. The effect of components other than horizontal tilt was very small since both linear regressions provided similar values. The smaller triangle symbols represent the case when a centered crystalline lens was incorporated into the modeling. Lens tilt with respect to the line of sight and lens decentration with respect to the pupil were both neglected. In this third case, a significant effect in the prediction of ocular coma was observed. The thinner line in the plot represents the linear regression. The correlation values did not provide any statistical meaning in this particular case. This indicates that most of the horizontal coma is produced by the particular horizontal misalignments of the ocular components.

The effect of a gradient index crystalline lens was also investigated. Figure 9 shows the prediction of coma with and without gradient index. The diamond shape symbols represent the ocular horizontal coma prediction for those models in the same conditions as explained before for Fig. 8 (the case with all misalignment data included), and the dashed line was the linear fit of these data, exactly as in Fig. 8. It must be stressed here that these lens models had a constant refractive index. In contraposition, the squared symbols represent the horizontal coma prediction from eye models that incorporated a gradient index lens. In this case, the Liu–Brennan lens model was the starting point for the optimization procedure to adjust the ocular SA, and the coefficients of the parabolic gradient index axial profile were also used as variables. The solid line represents the linear fit of the predicted data to the measured data ($R=0.79$, $p=0.0001$). Including a more sophisticated crystalline lens model with gradient index did not significantly increase the accuracy of the prediction since the data provided from both eye models were nearly the same.

It is important to note here that the internal aberrations generated with these individualized eye models were only internal aberrations due to the position of the lens with respect to the line of sight. It is also illustrative to compare the internal aberrations from the models (calculated as the subtraction of the corneal aberrations to the aberrations from the models) with the internal aberrations obtained from the measurements. These include both types of aberrations: intrinsic surface aberrations and angular generated aberrations. Figure 10 shows the results for both horizontal and vertical coma: For each of the subjects (x-axis), left positioned bars represent the

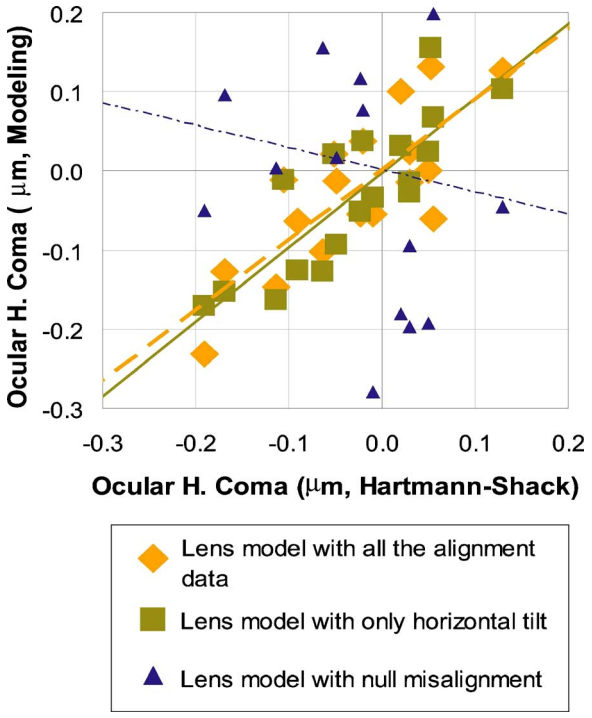

Fig. 8. (Color online) Influence of the crystalline lens alignment properties in the prediction of the horizontal coma of the eye (see text for details).

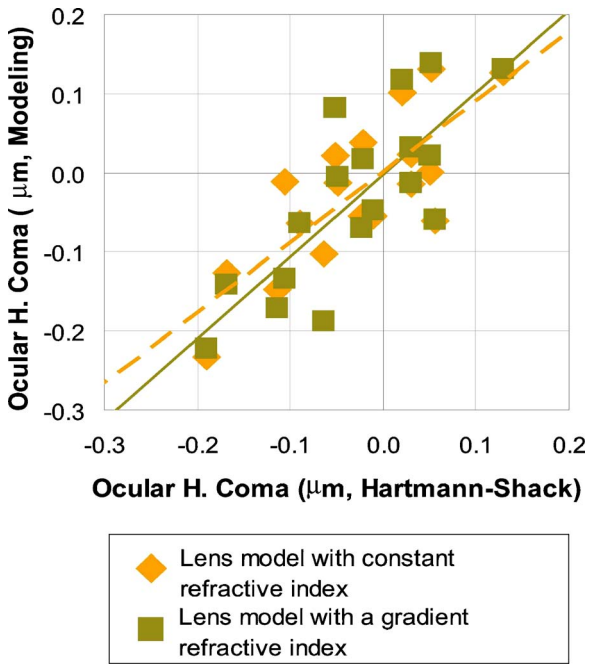

Fig. 9. (Color online) Influence of a gradient index crystalline lens model in the prediction of the horizontal coma of the eye (see text for details).

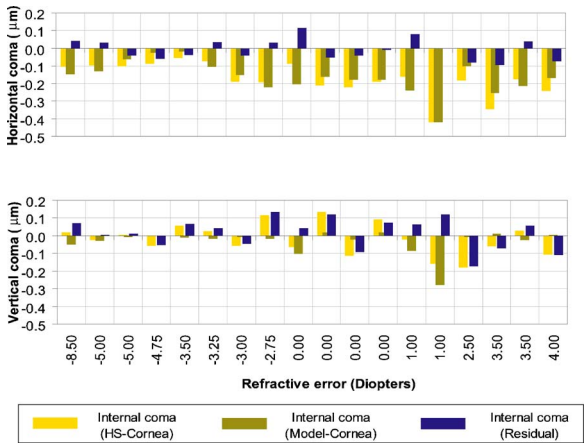

Fig. 10. (Color online) Measured internal total coma, angular generated internal coma, and residual internal coma for all the subjects included in the study, sorted by refractive error from myopic to hyperopic.

"total" internal coma obtained by direct subtraction of the measured corneal aberrations to the measured ocular aberrations; central bars represent the "angular" internal coma from the subtraction of the corneal aberrations to the ocular aberrations obtained with the modeling procedure, and right bars were the subtraction of the second (central) bar to the first (left) bar. An estimation of the intrinsic or structural aberrations of the lens, compared with the "angular" generated aberrations was obtained from this subtraction. In the case of horizontal coma, the agreement between the predicted angular aberrations and the total internal aberrations is quite high ($R=0.96$, $p<0.00001$). Therefore, the lens intrinsic horizontal coma is small (the right positioned bar for each subject in the upper panel of Fig. 10). In the case of vertical coma, the agreement between the predicted angular aberrations and the measured internal aberrations is not significant. These right positioned bars showed some values larger than those on the horizontal orientation. This result might indicate a more intrinsic component for this orientation of coma or, in others words, that the horizontal component of internal coma was due to the angular orientation of the crystalline lens, while vertical coma had mainly an intrinsic origin.

Other higher-order aberrations were not expected to be generated by the angular orientation of the lens. It is well known theoretically that coma is linearly dependent on the angular distance of the lens and the principal ray, but no other relations with the angular orientation are described for higher-order terms. The values for trefoil are shown in Fig. 11. In this case, the values of internal trefoil predicted by the models (central bars) are nearly zero, since the angular dependency of this aberration can be neglected. Therefore, trefoil is generated intrinsically within the lens surfaces (right bars) and no significant differences between the trefoil orientations were found.

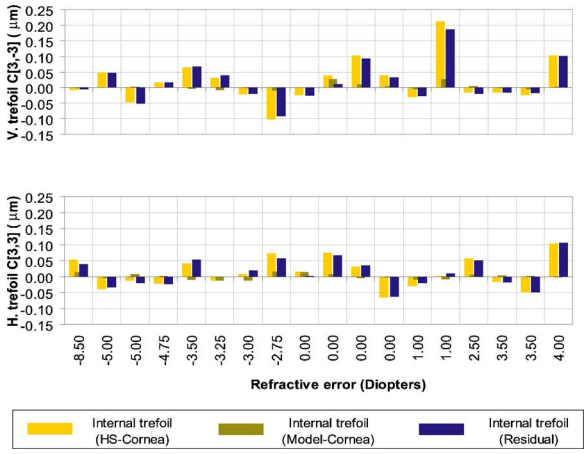

Fig. 11. (Color online) Measured internal total trefoil, angular generated internal trefoil, and residual internal trefoil for all subjects included in the study, sorted by refractive error from myopic to hyperopic.

4. DISCUSSION

The experimental data and modeling presented in this paper provided several important findings to help understand the mechanisms of compensation of optical aberrations between cornea and internal optics in the young human eye. As it has been previously described, corneal spherical aberration was confirmed to be higher than ocular SA, and this effect was not influenced by refractive error. The only optical mechanism responsible for this compensation can be formulated in terms of the asphericity of the crystalline lens surfaces or the gradient index of the crystalline lens. The compensation of the horizontal coma was found to have a significant dependence on refractive error. The optical modeling procedure can help understand this effect. First, the crystalline lens alignment parameters did not critically affect this compensation, with the important exception of the horizontal component of lens tilt. This component was mainly due to the horizontal angle kappa. And second, the gradient index has a minor impact in the ocular coma. It was also relevant that the remaining structural aberrations in the lens surfaces did not seem to be large and they did not change significantly with refractive error either.

One important question still remains: Why do corneal coma and lens coma have opposite signs? The answer is related to the typical field angle in the eye (the angle kappa), but the question that might be asked next is why this angle produces that effect.

A. Simple Optical Modeling of the Compensation Effect

To provide an explanation for the balance of coma in the human eye, it is important to understand the optical design of the eye and its basic components. The eye can be simplified as a two-lens optical system, the first lens of the system being a meniscus lens (the cornea), and the second lens being a biconvex lens (the crystalline lens). These two lenses are structurally different from each other since they have very different shape factors. Figure 12 illustrates the concept of shape factor [28] in a symmetrical index space. With this figure in mind, we can immediately recognize that the cornea must have a shape factor larger than 1, while the crystalline lens should have a shape factor between −1 and zero. Assuming a very simple rotationally symmetrical model, this optical system would not have coma unless a field angle was

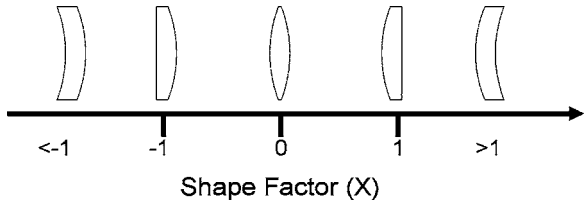

Fig. 12. Illustrative picture of the shape factor (X) concept in a symmetrical index space [$X=(R_1+R_2)/(R_1-R_2)$, R_1 and R_2 are the radii of curvature of the anterior and posterior surface of the lens].

present. However, these two lenses are immersed in a nonsymmetric refractive index media, from air to aqueous and from aqueous to vitreous, and the mathematical formulation differs from the situation when a symmetrical index space is present. An analytical expression for the Seidel coma of a thin lens immersed in a nonsymmetrical index space is given by [29]

$$A_c = -\frac{1}{4} n_1 h^3 K^2 \bar{u} [p_1 X^2 + p_2 Y^2 + p_3 XY + p_4 X + p_5 Y + p_6], \tag{1}$$

where n_1 is the refractive index of the object space, h is the height of the marginal ray at the lens, K is the lens power, $\bar{u}$ is the angle between the principal ray and the optical axis of the lens, the p_i factors are only functions of the refractive indexes of the media (tabulated in [29]) and X and Y are the shape and position factors defined as follows:

$$X = \frac{(n_L - n_1)R_2 + (n_L - n_2)R_1}{(n_L - n_1)R_2 - (n_L - n_2)R_1}, \tag{2}$$

$$Y = \frac{n_2 u' + n_1 u}{n_2 u' - n_1 u}. \tag{3}$$

n_L and n_2 are the refractive index of the lens and image space, R_1 and R_2 are the radii of curvature of the anterior and posterior surface of the lens, and u and u' are the incident and refracted angles of the marginal ray. Equation (1) reveals that for each fixed position factor, there are an infinite set of lens shapes with the same power but with different values for coma. The coma generated will be linear with the incident principal ray angle. A relationship between coma and shape factor can be derived for the cornea and the crystalline lens, introducing the value of the position factor Y on Eq. (1). For the cornea, since the object is assumed to be at infinity, the position factor is $Y_C = 1$; Eq. (1) can be rewritten as

$$Coma_C = -\frac{1}{4} h_C^3 K_C^2 \bar{u}_C [p_{1C} X_C^2 + (p_{3C} + p_{4C}) X_C + (p_{2C} + p_{5C} + p_{6C})]. \tag{4}$$

For the crystalline lens, under the assumption of equal refractive indexes for the aqueous and vitreous, some of the p factors are zero, and Eq. (1) can be rewritten in its more classical form (see [29]) as

$$Coma_L = -\frac{1.336}{4} h_L^3 K_L^2 \bar{u}_L [p_{4L} X_L + p_{5L} Y_L]. \tag{5}$$

The position factor for the lens Y_L can be calculated using Eq. (3) and simple paraxial optics with the geometry of the Gullstrand unaccomodated eye model. Assuming an aperture diameter of 5 mm, Eqs. (4) and (5) are plotted in Fig. 13 for different parameters: The parabolic curve represents the corneal coma as a function of its shape factor and the straight lines are the coma for the crystalline lens against shape factor. The three straight lines show coma for crystalline lenses of different powers: 15 D (solid line), 20 D (short dashed line), and 25 D (long dashed), respectively. The influence of corneal power was also evaluated but only small changes were found with little relevance to this discussion. The three panels represent the influence of the principal ray angle (equivalent to the field angle). Values of 2° (upper panel), 5° (medium panel), and 8° (lower panel) were used. Choosing any of the shape factors represented in the x-axis for each lens (cornea and crystalline), an optical system with similar first-order optical properties (optical power) to the eye could be selected, but, of course, a particular election of the actual shape factors will have tremendous implications on the third-order optical properties (third-order aberrations) and, in particular, in coma. Therefore the question that arises is what the shape factors are for conventional normal eyes. Using the Gullstrand cornea parameters, a value of shape factor of ~1.25 is obtained (plotted as a dot in the graphs). It is important to see that this shape factor generates a negative value for the corneal coma. For the crystalline lenses, the values for the shape factors are ~−0.25, providing a positive value for lens coma, opposite to corneal coma.

The fact that the corneal coma and crystalline lens have such different shapes is crucial to understanding the balance of ocular coma observed with the measurements. The optical design of the eye represents a natural (automatic) defense against the presence of field angles such as those naturally occurring in the eye, as the angle kappa or, if misalignments between the ocular components are neglected, angle alpha (the angle between the visual and best optical axis). These angular misalignments in the eye all have the same origin: The fovea is not located on the optical axis, but this proper shape design tends to attenuate what could have been a major optical imperfection. It is rather extraordinary to realize how the optical design of the human eye reassembles the characteristics of an aplanatic optical system, with the crystalline lens acting as an aspheric compensator to provide a (partial) correction of corneal spherical aberration and also with the proper choice of shapes to avoid a major generation of off-axis coma. Since angle kappa tends to be slightly larger for hyperopic eyes as compared with myopic eyes, it is expected to have a larger compensation effect for the hyperopic subjects. This prediction fit well with the experimental data presented in this paper (Fig. 2).

It must be mentioned that this treatment is strictly correct assuming that the stop-shift effect is neglected. In others words the coma plotted in Fig. 13 represents the corneal coma at the corneal plane with the cornea acting as its own stop aperture and also lens coma with the stop

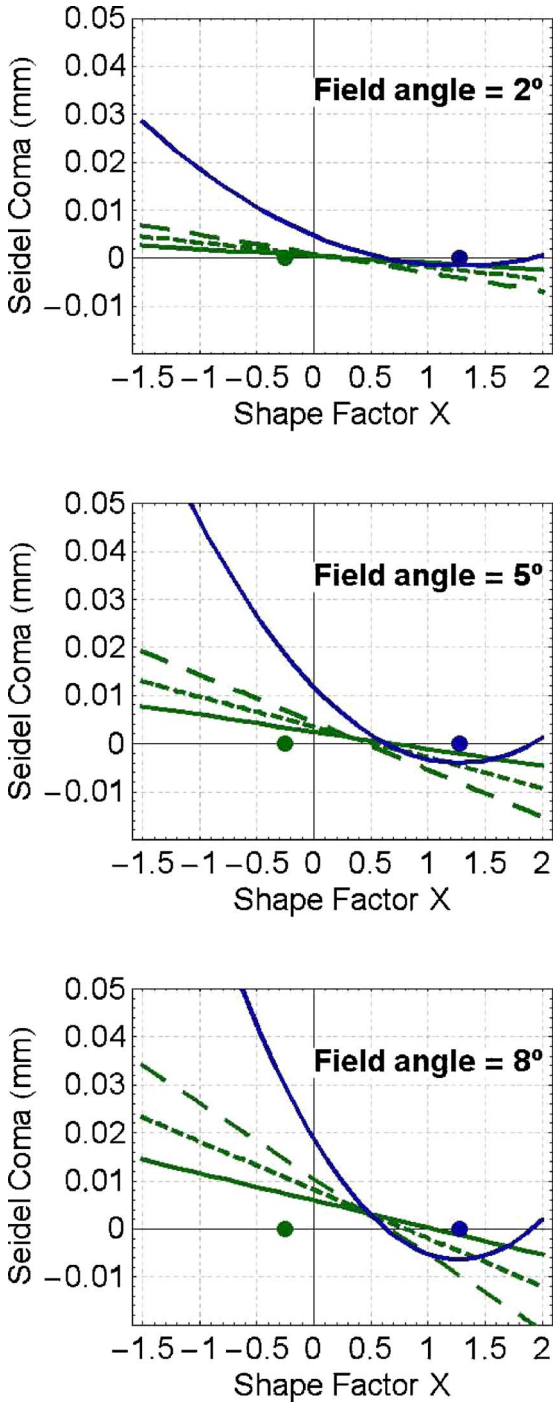

Fig. 13. (Color online) Corneal coma as function of shape factor (parabolic line) and lens coma as function of shape factor (straight lines) for three different principal ray angles (2° upper, 5° medium, and 8° lower panels) in the context of the simplified angular theory described in the text. Three different lens models were used (15, 20, and 25 diopters; see text for details). Dots represent the standard shape factor for a Gullstrand cornea model (1.25) and the standard shape factor for the Gullstrand crystalline lens model (−0.25).

aperture at its own plane. A strictly theoretical treatment of this problem represents a more complicated problem with little margin to improve the results. However, a ray-tracing procedure with the aperture stop (the physical pupil) placed in front of the lens, provided very similar results [12] to this simple theory (in terms of horizontal coma compensation).

Still, the pupil location in the eye has some surprising effects for ocular aberrations that are worth mentioning. Tilting the lens has, as has been described earlier, a linear effect in the generation of coma. One could object that this effect might be dependent on the spherical aberration of the surface. The following equation [30] describes the coefficient of Seidel coma generated due to the tilting effect of a lens with spherical aberration:

$$\delta Coma = -4sa_S\beta, \tag{5'}$$

where s is the distance from the exit pupil to the surface, a_S is the spherical aberration coefficient, and β is the angle of tilt of the surface. If the distance s can be neglected, there will be no coma generated by the asphericity of the surface. This is the case with the first crystalline lens surface. The physical pupil is placed against this surface, and the exit pupil of the eye is approximately at the same plane. Therefore, asphericity of the anterior lens surface has a minor effect on the generation of off-axis coma. Asphericity in the posterior surface might have some effect, but in any case this is an additive quantity to the linear coma generated by obliquity in spherical surfaces and it would contribute as a noisy source to the compensation effect (imperfect correlations in Fig. 7 might indicate the presence of some noisy sources).

B. Elongation Model of the Eye Versus Angle Kappa

The actual shapes of the components of the eye produce a large coma compensation effect in the presence of typical ocular field angles. This effect is more important in hyperopic subjects since they tend to have a larger angle kappa than myopic eyes. It might be interesting to explore in detail the reason for this tendency. This can be explained by a simple model of the axial growing of the eye. It is well known that one of the mechanisms for the development of myopia is an abnormal axial growth of the eye. Magnetic resonance images have clearly shown that this kind of myopia is prevalent among the myopic population [31]. Therefore, it is expected that the fovea would remain relatively unchanged in its vertical position with little migration in this direction, since the main growing of the eye is axial. Assuming this foveal position is stable in the growing eye [see Fig. 14(a)] and also that the change in the approximate nodal points of the eye is small in comparison with the change in the axial position of the retina, we can formulate a simple model of how angle kappa might

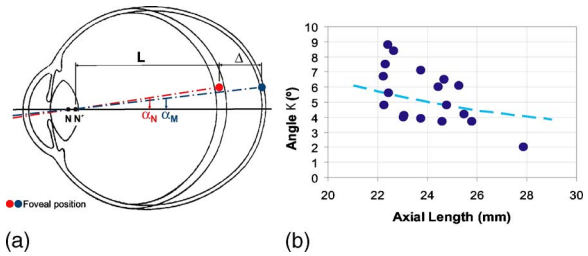

Fig. 14. (Color online) (a) Schematic geometry of the elongation model of an eye from normal to myopic refractive states. (b) Angle kappa measured as a function of the axial length (dots) and the theoretical prediction of a simple geometrical model of eye elongation (dashed line).

change with the axial length of the eye. Let Δ and L represent this change and the distance from the nodal image point to the retina, respectively. The field angle presented in the eye (the angle between the optical axes in this ideal case and the visual axes) is denoted as α. In the normal emmetrope subject we called it α_N. Using simple geometry, from Fig. 14(a) we could express the field angle when the eye grows an axial magnitude of Δ as

$$\alpha_M = \tan^{-1}\left[\left(\frac{L}{L+\Delta}\right)\tan(\alpha_N)\right]. \quad (6)$$

The starting point is an average normal emmetropic eye with an axial length of 24 mm, $\alpha_N = 5$ degrees, and $L = 16.5$ mm. Figure 14(b) shows the prediction of the angle, using Eq. (6) as the eye becomes longer and shorter (dashed curve) together with our measured data on axial length and angle kappa. The variation among subjects is large and probably there are important individual differences with this simple model. However, the tendency obtained through this equation is useful for explaining (at least partially) the influence of eye elongation for angle kappa.

C. Compensation Mechanisms Render a Robust Eye Design

The model proposed in this paper is strictly related to the angular generated coma. It seems that the intrinsic components of coma associated with the crystalline surfaces are small as compared with the angular component, at least for the horizontal projection of coma. However, although the corneal coma tended to have a very significant angular component, in some cases the intrinsic structural aberration was even stronger than the angular generated coma and it should not be neglected at all. Figure 7 showed this relation. If corneal coma was entirely generated by the angular value, a perfect linear relation should be expected for the diamond shape symbols. Although this relation was very significant, some points were scattered around, which revealed the presence of a structural intrinsic coma independent of the angle.

Some interesting new questions may arise beyond the scope of this current paper. Although the shapes of the crystalline lens change with age, they do not change enough to significantly modify its shape factor, and similarly for the cornea. Therefore, the balance of ocular coma with age relies on the temporal evolution of angle kappa and we believe that no works have been performed on this topic so far. It would also be interesting to study the change of shape and position factors on the aberrations during accommodation. All the theory and measurements performed in this study are valid in the unaccommodated range when the subject fixates to a far target. However, changing the accommodation level would modify the position factor for the cornea, and also the shape factor for the lens. This fact by itself would predict a modification in the ocular coma. The alignment properties might also play a role in the accommodation dynamics if the line of sight tends to change with the accommodation amplitude.

These series of experiments and optical modeling allowed us to understand the basic mechanisms of the optical design in the human eye. We showed that the eye behaves in a similar way as an aplanatic optical system. This is a much optimized design solution rendering a very stable retinal image quality for a variety of geometrical configurations: axial longitude or ocular misalignment.

In summary, the results presented here have provided, for what we believe is the first time, a convincing explanation for the balance of aberrations, and in particular the balance of the horizontal coma in the normal young eye. The role of the alignment properties in the eye has been studied and measured in detail, and some aspects that had not yet been understood have been explained and successfully modeled.

ACKNOWLEDGMENTS

This research was supported in part by the Spanish Ministerio de Educación y Ciencia (grant FIS2004-2153 to P. A.).

REFERENCES AND NOTES

1. S. G. El Hage and F. Berny, "Contribution of the crystalline lens to the spherical aberration of the eye," J. Opt. Soc. Am. **63**, 205–211 (1973).
2. P. Artal and A. Guirao, "Contribution of cornea and lens to the aberrations of the human eye," Opt. Lett. **23**, 1713–1715 (1998).
3. P. Artal, A. Guirao, E. Berrio, and D. R. Williams, "Compensation of corneal aberrations by the internal optics in the human eye," J. Vision **1**, 1–8 (2001).
4. P. Artal, E. Berrio, A. Guirao, and P. Piers, "Contribution of the cornea and internal surfaces to the change of ocular aberrations with age," J. Opt. Soc. Am. **19**, 137–143 (2002).
5. A. Glasser and M. C. W. Campbell, "Presbyopia and the optical changes in the human crystalline lens with age," Vision Res. **38**, 209–229 (1998).
6. A. Guirao, M. Redondo, and P. Artal, "Optical aberrations of the human cornea as a function of age," J. Opt. Soc. Am. A **7**, 1697–1702 (2000).
7. A. Guirao, M. Redondo, E. Geraghty, P. Piers, S. Norrby, and P. Artal, "Corneal optical aberrations and retinal image quality in patients in whom monofocal intraocular lenses were implanted," Arch. Ophthalmol. (Chicago) **120**, 1143–1151 (2002).
8. J. T. Holladay, P. A. Piers, G. Koranyi, M. van der Mooren, and N. E. Norrby, "A new intraocular lens design to reduce spherical aberration of pseudophakic eyes," J. Refract. Surg. **18**, 683–691 (2002).
9. U. Mester, P. Dillinger, and N. Anterist, "Impact of a modified optic design on visual function: clinical comparative study," J. Cataract Refractive Surg. **29**, 652–660 (2003).
10. R. Bellucci, A. Scialdone, L. Buratto, S. Morselli, C. Chierego, A. Criscouli, G. Moretti, and P. Piers, "Visual acuity and contrast sensitivity comparison between Tecnis and AcrySof SA60AT intraocular lenses: A multicenter randomized study," J. Cataract Refractive Surg. **31**, 712–717 (2005).
11. J. E. Kelly, T. Mihashi, and H. C. Howland, "Compensation of corneal horizontal/vertical astigmatism, lateral coma, and spherical aberration by internal optics of the eye," J. Vision **4**, 262–271 (2004).
12. P. Artal, A. Benito, and J. Tabernero, "The human eye is an example of robust optical design," J. Vision **6**, 1–7 (2006).
13. Y. Le Grand and S. G. El Hage, *Physiological Optics* (Springer Series in Optical Sciences, 1980).
14. The same angle formed by the line of sight and the pupillary axis is referred to in the literature with two different names: for instance, kappa in [13] and lambda in [15] and others. The reason for this notation discrepancy can be found in the historical references and the intrinsic

confusion with ocular angle definitions. In the clinical literature only kappa is commonly used, while lambda is still used by some basic researchers. According to Emsley [16], the first definition of angle kappa was given by Landolt as "the angle between the visual axis and the so-called central pupillary line (the pupillary axis)." This definition involved the visual axis, as the line connecting the fixation point with the object nodal point of the eye. This is not the same as the line of sight, connecting the center of the entrance pupil and the fixation point. Therefore this definition is not what was used by Le Grand and adopted here. Angle lambda was defined by Lancaster (cited in [13]) as the line connecting the pupillary axis and the line of sight. However, Le Grand and El Hage [13] redefined angle kappa exactly as the angle lambda defined by Lancaster. The reason to do this is that they understand the term "visual axis" in Landolt's original definition of kappa as the line of sight, since the nodal point in the eye is a purely paraxial theoretical concept that cannot be measured. Quoting Le Grand's book, p. 73: "It is not very logical to confuse geometric and fictitious ideas (optical and visual axis) and experimental ideas (pupillary axis and the principal line of sight)." Therefore, Le Grand maintained the old name of kappa but with the modern definition of lambda by Lancaster. Moreover, in practical terms, the two angles are nearly identical as stated by Le Grand [13]: "It seems unnecessary to distinguish this (angle lambda) from kappa which is practically equal to it when the point of fixation is not very close to the eye." We used in the manuscript this meaning for angle kappa, but the reader should be aware of the other accepted name (lambda) for the same angle to avoid confusion. A standard definition of ocular angles is required to unify terms in both basic and clinical literature. In the case of this angle, keeping only the name kappa would be, in our opinion, the most adequate.

15. D. A. Atchison and G. Smith, *Optics of the Human Eye* (Butterworth-Heineman, 2000).
16. H. H. Emsley, *Visual Optics* (Hatton Press, 1948).
17. J. Tabernero, P. Piers, and P. Artal, "Intraocular lens to correct corneal coma," Opt. Lett. **32**, 406–408 (2007).
18. D. L. Guyton, H. Uozato, and H. J. Wisnicki, "Rapid determination of intraocular lens tilt and decentration through the undilated pupil," Ophthalmologica **97**, 1259–1264 (1990).
19. J. C. Barry, M. C. M. Dunne, and T. Kirschkamp, "Phakometric measurement of ocular surface radius of curvature and alignment: evaluation of method with physical model eyes," Ophthalmic Physiol. Opt. **21**, 450–460 (2001).
20. P. Rosales and S. Marcos, "Phokometry and lens tilt and decentration using a custom-developed Purkinje imaging apparatus: validation and measurements," J. Opt. Soc. Am. A **23**, 509–520 (2006).
21. J. Tabernero, A. Benito, V. Nourrit, and P. Artal, "Instrument for measuring the misalignments of ocular surfaces," Opt. Express **14**, 10945–10956 (2006).
22. H. Howland, A. Glasser, and R. Applegate, "Polynomial approximations of corneal surfaces and corneal curvature topography," Tech. Dig. Ser. Opt. Soc. Am. **3**, 34–37 (1992).
23. A. Guirao and P. Artal, "Corneal wave aberration from videokeratography: accuracy and limitations of the procedure," J. Opt. Soc. Am. A **17**, 955–965 (2000).
24. J. C. Liang, B. Grimm, S. Goelz, and J. F. Bille, "Objective measurement of wave aberrations of the human eye with the use of a Hartmann–Shack wave-front sensor," J. Opt. Soc. Am. A **11**, 1949–1957 (1994).
25. P. M. Prieto, F. Vargas-Martín, S. Goelz, and P. Artal, "Analysis of the performance of the Hartmann-Shack sensor in the human eye," J. Opt. Soc. Am. A **17**, 1388–1398 (2000).
26. J. Tabernero, P. Piers, A. Benito, M. Redondo, and P. Artal, "Predicting the optical performance of eyes implanted with IOLs correcting spherical aberration," Invest. Ophthalmol. Visual Sci. **47**, 4651–4658 (2006).
27. H. L. Liou and N. A. Brennan, "Anatomically accurate, finite model eye for optical modelling," J. Opt. Soc. Am. A **14**, 1684–1695 (1997).
28. V. N. Mahajan, *Aberration Theory Made Simple* (SPIE, 1991).
29. L. N. Hazra and C. A. Delisle, "Primary aberrations of a thin lens with different object and image space media," J. Opt. Soc. Am. A **15**, 945–953 (1998).
30. V. N. Mahajan, *Optical Imaging and Aberrations. Part I. Ray Geometrical Optics* (SPIE, 1998).
31. D. A. Atchison, C. E. Jones, K. L. Schmid, N. Prichard, J. M. Pope, W. E. Strugnell, and R. A. Riley, "Eye shape in emmetropia and myopia," Invest. Ophthalmol. Visual Sci. **45**, 3380–3386 (2004).